International Tables for Crystallography (2010). Vol. B, Chapter 5.3, pp. 654–664.

5.3. Dynamical theory of neutron diffraction

By M. Schlenker and J.-P. Guigay

5.3.1. Introduction

Neutron and X-ray scattering are quite similar both in the geometry of scattering and in the orders of magnitude of the basic quantities. When the neutron spin is neglected, *i.e.* when dealing with scattering by perfect nonmagnetic crystals, the formalism and the results of the dynamical theory of X-ray scattering can be very simply transferred to the case of neutrons (Section 5.3.2). Additional features of the neutron case are related to the neutron spin and appear in diffraction by magnetic crystals (Section 5.3.3). The low intensities available, coupled with the low absorption of neutrons by most materials, make it both necessary and possible to use large samples in standard diffraction work. The effect of extinction in crystals that are neither small nor bad enough to be amenable to the kinematical approximation is therefore very important in the neutron case, and will be discussed in Section 5.3.4 together with the effect of crystal distortion. Additional possibilities arise in the neutron case because the neutrons can be manipulated from outside through applied fields (Section 5.3.5). Reasonably extensive tests of the predictions of the dynamical theory of neutron diffraction have been performed, with the handicap of the very low intensities of neutron beams as compared with X-rays: these are described in Section 5.3.6. Finally, the applications of the dynamical theory in the neutron case, and in particular neutron interferometry, are reviewed in Section 5.3.7.

5.3.2. Comparison between X-rays and neutrons with spin neglected

5.3.2.1. The neutron and its interactions

An excellent introductory presentation of the production, properties and scattering properties of neutrons is available (Scherm & Fåk, 1993, and other papers in the same book). A stimulating review on neutron optics, including diffraction by perfect crystals, has been written by Klein & Werner (1983). X-rays and neutrons are compared in terms of the basic quantities in Table 4.1.3.1 of *IT* C (2004), where Chapter 4.4 is devoted to neutron techniques.

The neutron is a massive particle for which the values relevant to diffraction are: no electric charge, rest mass $m = 1.675 \times 10^{-27}$ kg, angular momentum eigenvalues along a given direction $\pm\hbar/2$ (spin $\frac{1}{2}$) and a magnetic moment of -1.913 nuclear magneton, meaning that its component along a quantization direction z can take eigenvalues $\mu_z = \mp 0.996 \times 10^{-26}$ A m^2. The de Broglie wavelength is $\lambda = h/p$ where h is Planck's constant ($h = 2\pi\hbar = 6.625 \times 10^{-34}$ J s) and p is the linear momentum; $p = mv$ in the nonrelativistic approximation, which always applies in the context of this chapter, v being the neutron's velocity. The neutron's wavelength, λ, and kinetic energy, E_c, are thus related by $\lambda = h/(2mE_c)^{1/2}$, or, in practical units, $\lambda\,[\text{Å}] = 9.05/(E_c\,[\text{meV}])^{1/2}$. Thus, to be of interest for diffraction by materials, neutrons should have kinetic energies in the range 10^0 to 10^2 meV. In terms of the velocity, $\lambda\ [\text{Å}] = 3.956/(v\ [\text{km s}^{-1}])$.

Neutron beams are produced by nuclear reactors or by spallation sources, usually pulsed. In either case they initially have an energy in the MeV range, and have to lose most of it before they can be used. The moderation process involves inelastic interactions with materials. It results in statistical distributions of energy, hence of velocity, close to the Maxwell distribution characteristic of the temperature T of the moderator. Frequently used moderators are liquid deuterium (D_2, *i.e.* $^2H_2$) at 25 K, heavy water (D_2O) at room temperature and graphite allowed to heat up to 2400 K; the corresponding neutron distributions are termed cold, thermal and hot, respectively.

The interaction of a neutron with an atom is usually described in terms of scattering lengths or of scattering cross sections. The main contribution corresponding to the nuclear interaction is related to the strong force. The interaction with the magnetic field created by atoms with electronic magnetic moments is comparable in magnitude to the nuclear term.

5.3.2.2. Scattering lengths and refractive index

The elastic scattering amplitude for scattering vector $\mathbf{s}$, $f(\mathbf{s})$, is defined by the wave scattered by an object placed at the origin when the incident plane wave is $\Psi_i = A\exp[i(\mathbf{k}_0\cdot\mathbf{r} - \omega t)]$, written as $\Psi_s = A[f(\mathbf{s})/r]\exp[i(kr - \omega t)]$ with $k = |\mathbf{k}_0| = |\mathbf{k}_0 + \mathbf{s}| = 2\pi/\lambda$. In the case of the strong-force interaction with nuclei, the latter can be considered as point scatterers because the interaction range is very small, hence the scattering amplitude is isotropic (independent of the direction of $\mathbf{s}$). It is also independent of λ except in the vicinity of resonances. It is conventionally written as $-b$ so that most values of b, called the scattering length, are positive. A table of experimentally measured values of the scattering lengths b is given in *IT* C for the elements in their natural form as well as for many individual isotopes. It is apparent that the typical order of magnitude is the fm (femtometre, *i.e.* 10^{-15} m, or fermi), that there is no systematic variation with atomic number and that different isotopes have very different scattering lengths, including different signs. The first remark implies that scattering amplitudes of X-rays and of neutrons have comparable magnitudes, because the characteristic length for X-ray scattering (the scattering amplitude for forward scattering by one free electron) is $R = 2.8$ fm, the classical electron radius. The second and third points explain the importance of neutrons in structural crystallography, in diffuse scattering and in small-angle scattering. Scattering of neutrons by condensed matter implies the use of the bound scattering lengths, as tabulated in *IT* C. The 'free' scattering length, used in some presentations, is obtained by multiplying the bound scattering lengths by $A/(A+1)$, where A is the mass of the nucleus in atomic units.

A description in terms of an interaction potential is possible using the Fermi pseudo-potential, which in the case of the nuclear interaction with a nucleus at $\mathbf{r}_0$ can be written as $V(\mathbf{r}) = (h^2/2\pi m)b\delta(\mathbf{r} - \mathbf{r}_0)$, where δ denotes the three-dimensional Dirac distribution.

Refraction of neutrons at an interface can be conveniently described by assigning a refractive index to the material, such that the wavenumber in the material, k, is related to that in a vacuum, k_0, by $k = nk_0$. Here

$$n = \left(1 - \frac{\lambda^2}{\pi V}\sum_i b_i\right)^{1/2},$$

where the sum is over the nuclei contained in volume V. With typical values, n is very close to 1 and $1 - n = (\lambda^2/2\pi V)\sum_i b_i$ is

typically of the order of 10^{-5}. This small value, in the same range as for X-rays, gives a feeling for the order of magnitude of key quantities of the dynamical theory, in particular the Darwin width 2δ as discussed in Chapter 5.1. It also makes total external reflection possible on materials for which $\sum_i b_i > 0$: this is the basis for the neutron guide tubes now installed in most research reactors, as well as for reflectometry.

The notations prevailing in X-ray and in neutron crystallography are slightly different, and the correspondence is very simple: X-ray atomic scattering factors and structure factors are numbers. When multiplied by R, the classical electron radius, they become entirely equivalent to the corresponding quantities in neutron usage, which are lengths. It should be noted that the presence of different isotopes and the effect of nuclear spin (disordered except under very special conditions) give rise to incoherent elastic neutron scattering, which has no equivalent in the X-ray case. The scattering length corresponding to R times the atomic scattering factor for X-rays is therefore the coherent scattering length, $b_{\rm coh}$, obtained by averaging the scattering length over the nuclear spin state and isotope distribution.

5.3.2.3. Absorption

Neutron absorption is related to a nuclear reaction in which the neutron combines with the absorbing nucleus to form a compound nucleus, usually in a metastable state which then decays. The scattering length describing this resonance scattering process depends on the neutron energy and contains an imaginary part associated with absorption in complete analogy with the imaginary part of the dispersion correction for the X-ray atomic scattering factors. The energies of the resonances are usually far above those of interest for crystallography, and the linear absorption coefficient varies approximately as $1/v$ or λ. It is important to note that, except for a very few cases (notably ^{3}He, ^{6}Li, ^{10}B, In, Cd, Gd), the absorption of neutrons is very small compared with that of X-rays, and even more so compared with that of electrons, and can be neglected to a first approximation.

5.3.2.4. Differences between neutron and X-ray scattering

There are major differences in the experimental aspects of neutron and X-ray scattering. Neutrons are only available in large facilities, where allocation of beam time to users is made on the basis of applications, and where admittance is restricted because of the hazards which nuclear technology can present in the hands of ill-intentioned users. Because of the radiation shielding necessary, as well as the large size of neutron detectors, neutron-scattering instrumentation is much bulkier than that for X-rays. Neutron beams are in some aspects similar to synchrotron radiation, in particular because in both cases the beams are initially 'white' and for most applications have to be monochromated. There is, however, a huge difference in the order of magnitudes of the intensities. Neutron beams are weak in comparison with laboratory X-ray sources, and weaker by many orders of magnitude than synchrotron radiation. Also, the beam sources are large in the case of neutrons, since they are essentially the moderators, whereas the source is very small in the case of synchrotron radiation, and this difference again increases the ratio of the brilliances in favour of X-rays. This encourages the use of large specimens in all neutron-scattering work, and makes the extinction problem more important than for X-rays. Furthermore, many experiments that are quick using X-rays become very slow, and give rise to impaired resolution, in the neutron case.

There are also at least two additional aspects of neutron scattering in comparison with X-ray scattering, apart from the effect of the magnetic moment associated with the intrinsic (spin) angular momentum of the neutron. On the one hand, the small velocity of neutrons, compared with the velocity of light, makes time-of-flight measurements possible, both in standard neutron diffraction and in investigations of perfect crystals. Because this velocity is of the same order of magnitude as that of ultrasound, the effect of ultrasonic excitation on neutron diffraction is slightly different from that in the X-ray case. On the other hand, the fact that neutrons have mass and a magnetic moment implies that they can be affected by external fields, such as gravity and magnetic fields, both during their propagation in air or in a vacuum and while being diffracted within crystals (Werner, 1980) (see Section 5.3.5). Experiments completely different from the X-ray case can thus be performed with perfect crystals and with neutron interferometers (see Sections 5.3.6 and 5.3.7.3).

5.3.2.5. Translating X-ray dynamical theory into the neutron case

As shown in Chapter 5.1, the basic equations of dynamical theory, *viz* Maxwell's equations for the X-ray case and the time-independent Schrödinger equation in the neutron case, have exactly the same form when the effect of the neutron spin can be neglected, *i.e.* in situations that do not involve magnetism and when no externally applied potential is taken into account. The translation scheme for the scattering factors and structure factors is described above. The one formal difference is that the wavefunction is scalar in the neutron case, hence there is no equivalent to the parallel and perpendicular polarizations of the X-ray situation: C in equation (5.1.2.20) of Chapter 5.1 should therefore be set to 1.

The physics of neutron diffraction by perfect crystals is therefore expected to be very similar to that of X-ray diffraction, with the existence of wavefields, *Pendellösung* effects, anomalous transmission, intrinsic rocking-curve shapes and reflectivity *versus* thickness behaviour in direct correspondence. All experimental tests of these predictions confirm this view (Section 5.3.6).

Basic discussions of dynamical neutron scattering are given by Stassis & Oberteuffer (1974), Sears (1978), Rauch & Petrascheck (1978) and Squires (1978).

5.3.3. Neutron spin, and diffraction by perfect magnetic crystals

5.3.3.1. Polarization of a neutron beam and the Larmor precession in a uniform magnetic field

A polarized neutron beam is represented by a two-component spinor,

$$|\varphi\rangle = \begin{pmatrix} c \\ d \end{pmatrix} = c\begin{pmatrix} 1 \\ 0 \end{pmatrix} + d\begin{pmatrix} 0 \\ 1 \end{pmatrix},$$

which is the coherent superposition of two states, of different amplitudes c and d, polarized in opposite directions along the spin-quantization axis. The spinor components c and d are generally space- and time-dependent. We suppose that $\langle\varphi|\varphi\rangle = cc^* + dd^* = 1$. The polarization vector $\mathbf{P}$ is defined as

$$\mathbf{P} = \langle\varphi|\boldsymbol{\sigma}|\varphi\rangle,$$

where the vector $\boldsymbol{\sigma}$ represents the set of Pauli matrices σ_x, σ_y and σ_z. The components of $\mathbf{P}$ are

$$\begin{aligned} P_x &= \begin{pmatrix} c^* & d^* \end{pmatrix}\sigma_x \begin{pmatrix} c \\ d \end{pmatrix} = \begin{pmatrix} c^* & d^* \end{pmatrix}\begin{pmatrix} 0 & 1 \\ 1 & 0 \end{pmatrix}\begin{pmatrix} c \\ d \end{pmatrix} \\ &= c^*d + cd^* \\ P_y &= \begin{pmatrix} c^* & d^* \end{pmatrix}\sigma_y \begin{pmatrix} c \\ d \end{pmatrix} = \begin{pmatrix} c^* & d^* \end{pmatrix}\begin{pmatrix} 0 & -i \\ i & 0 \end{pmatrix}\begin{pmatrix} c \\ d \end{pmatrix} \\ &= i(cd^* - c^*d) \\ P_z &= \begin{pmatrix} c^* & d^* \end{pmatrix}\sigma_z \begin{pmatrix} c \\ d \end{pmatrix} = \begin{pmatrix} c^* & d^* \end{pmatrix}\begin{pmatrix} 1 & 0 \\ 0 & -1 \end{pmatrix}\begin{pmatrix} c \\ d \end{pmatrix} \\ &= cc^* - dd^*, \end{aligned} \tag{5.3.3.1}$$

from which it is clearly seen that, unlike P_z, the polarization components P_x and P_y depend on the phase difference between the spinor components c and d.

In a region of a vacuum in which a uniform magnetic field $\mathbf{B}$ is present, a neutron beam experiences a magnetic potential energy represented by the matrix

$$-\mu_n \boldsymbol{\sigma}\cdot\mathbf{B} = \begin{pmatrix} -\mu_n B & 0 \\ 0 & \mu_n B \end{pmatrix},$$

μ_n being the neutron magnetic moment, if the directions of $\mathbf{B}$ and of the spin-quantization axis coincide. Consequently, different indices of refraction $n = 1 \pm (\mu_n B/2E)$, where E is the neutron energy, should be associated with the spinor components c and d; this induces between these spinor components a phase difference which is a linear function of the time (or, equivalently, of the distance travelled by the neutrons), hence, according to (5.3.3.1), a rotation around the magnetic field of the component of the neutron polarization perpendicular to this magnetic field. The time frequency of this so-called Larmor precession is $2\mu_n B/h$, where h is Planck's constant.

A neutron beam may be partially polarized; such a beam is conveniently represented by a spin-density matrix ρ, which is the statistical average of the spin-density matrices associated to the polarized beams which are mixed incoherently, the density matrix associated to the spinor

$$|\varphi\rangle = \begin{pmatrix} c \\ d \end{pmatrix}$$

being

$$|\varphi\rangle\langle\varphi| = \begin{pmatrix} c \\ d \end{pmatrix}\begin{pmatrix} c^* & d^* \end{pmatrix} = \begin{pmatrix} cc^* & cd^* \\ c^*d & dd^* \end{pmatrix}.$$

The polarization vector $\mathbf{P}$ is then obtained as

$$\mathbf{P} = \mathrm{Tr}(\boldsymbol{\sigma}\rho). \tag{5.3.3.2}$$

In the common case of a nonpolarized beam, the spin-density matrix is

$$\rho = \tfrac{1}{2}\begin{pmatrix} 1 & 0 \\ 0 & 1 \end{pmatrix}.$$

It is easily seen that all components of $\mathbf{P}$ are then equal to 0.

Equation (5.3.3.2) is therefore applicable to the general case (polarized, partially polarized or nonpolarized beam). The inverse relation giving the density matrix ρ as function of $\mathbf{P}$ is

$$\rho = \tfrac{1}{2}\begin{pmatrix} 1 & 0 \\ 0 & 1 \end{pmatrix} + \tfrac{1}{2}\mathbf{P}\cdot\boldsymbol{\sigma}. \tag{5.3.3.3}$$

5.3.3.2. Magnetic scattering by a single ion having unpaired electrons

The spin and orbital motion of unpaired electrons in an atom or ion give rise to a surrounding magnetic field $\mathbf{B}(\mathbf{r})$ which acts on the neutron *via* the magnetic potential energy $-\boldsymbol{\mu}_n\cdot\mathbf{B}(\mathbf{r})$, where $\boldsymbol{\mu}_n$ is the neutron magnetic moment. Since this is a long-range interaction, in contrast to the nuclear interaction, the magnetic scattering length p, which is proportional to the Fourier transform of the magnetic potential energy distribution $-\boldsymbol{\mu}_n\cdot\mathbf{B}(\mathbf{r})$, depends on the angle of scattering.

The classical relation $\mathrm{div}\ \mathbf{B}(\mathbf{r}) = 0$ shows clearly that the vector $\mathbf{B}(\mathbf{s})$, which is the Fourier transform of $\mathbf{B}(\mathbf{r})$, is perpendicular to the reciprocal-space vector $\mathbf{s}$. If we consider the magnetic field $\mathbf{B}(\mathbf{r})$ as resulting from a point-like magnetic moment $\boldsymbol{\mu}$ at position $\mathbf{r} = 0$, we get

$$\mathbf{B}(\mathbf{r}) = \frac{\mu_0}{4\pi}\mathrm{curl}\frac{\boldsymbol{\mu}\times\mathbf{r}}{r^3},$$

where $\mu_0 = 4\pi \times 10^{-7}$ H m^{-1} is the permittivity of a vacuum and $\times$ denotes the cross product. $\mathbf{B}(\mathbf{r})$ can be Fourier-transformed into

$$\mathbf{B}(\mathbf{s}) = \mu_0\mathbf{s}\times\frac{\boldsymbol{\mu}\times\mathbf{s}}{s^2} = \mu_0\boldsymbol{\mu}_\perp(\mathbf{s}), \tag{5.3.3.4}$$

where $\boldsymbol{\mu}_\perp(\mathbf{s})$ is the projection of $\boldsymbol{\mu}$ on the plane perpendicular to $\mathbf{s}$ (reflecting plane).

This result can be applied by volume integration to the more general case of a spatially extended magnetization distribution, which for a single magnetic ion corresponds to the atomic shell of the unpaired electrons. It is thus shown that the magnetic scattering length is proportional to $\boldsymbol{\mu}_n\cdot\boldsymbol{\mu}_{i\perp}$, where $\boldsymbol{\mu}_{i\perp}$ is the projection of the magnetic moment of the ion on the reflecting plane.

For a complete description of magnetic scattering, which involves the spin-polarization properties of the scattered beam, it is necessary to represent the neutron wavefunction in the form of a two-component spinor and the ion's magnetic moment as a spin operator which is a matrix expressed in terms of the Pauli matrices $\boldsymbol{\sigma}$ $(\sigma_x, \sigma_y, \sigma_z)$. The magnetic scattering length is therefore itself a (2×2) matrix:

$$(\mathrm{p}) = -(2\pi m/h^2)\mu_n\boldsymbol{\sigma}\cdot\mathbf{B}(\mathbf{s}) = -\mu_0(2\pi m/h^2)\mu_n\boldsymbol{\sigma}\cdot\boldsymbol{\mu}_{i\perp}(\mathbf{s})f_i(\sin\theta/\lambda), \tag{5.3.3.5}$$

where $f_i(\sin\theta/\lambda)$ is the dimensionless magnetic form factor of the ion considered and tends towards a maximum value of 1 when the scattering angle θ tends towards 0 (forward scattering). The value of $\mu_0(2\pi m/h^2)\mu_n\mu_i$ is $p_1 = 2.70 \times 10^{-15}$ m for $\mu_i = 1$ Bohr magneton.

According to (5.3.3.4) or (5.3.3.5), there is no magnetic scattering in directions such that the scattering vector $\mathbf{s}$ is in the same direction as the ion magnetic moment $\boldsymbol{\mu}_i$. Magnetic scattering effects are maximum when $\mathbf{s}$ and $\boldsymbol{\mu}_i$ are perpendicular.

The matrix (p) is diagonal if the direction of $\boldsymbol{\mu}_{i\perp}(\mathbf{s})$ is chosen as the spin-quantization axis. Therefore, there is no spin-flip scattering if the incident beam is polarized parallel or antiparallel to the direction of $\boldsymbol{\mu}_{i\perp}(\mathbf{s})$.

It is more usual to choose the spin-quantization axis (Oz) along $\boldsymbol{\mu}_i$. Let β be the angle between the vectors $\boldsymbol{\mu}_i$ and $\mathbf{s}$; the

(x, y, z) components of $\boldsymbol{\mu}_{i\perp}(\mathbf{s})$ are then $(-\mu_i \sin\beta\cos\beta,\ 0,\ \mu_i \sin^2\beta)$ if the y axis is chosen along $\boldsymbol{\mu}_i \times \mathbf{s}$. The total scattering length, which is the sum of the nuclear and the magnetic scattering lengths, is then represented by the matrix

$$(\mathrm{q}) = \begin{pmatrix} b + p\sin^2\beta & -p\sin\beta\cos\beta \\ -p\sin\beta\cos\beta & b - p\sin^2\beta \end{pmatrix}, \qquad (5.3.3.6)$$

where b is the nuclear scattering length and

$$p = -\mu_0 \frac{2\pi m}{h^2} \mu_n \mu_i f_i\left(\frac{\sin\theta}{\lambda}\right) = -p_1 \mu_i f_i\left(\frac{\sin\theta}{\lambda}\right),$$

with μ_i expressed in Bohr magnetons. The relations

$$(\mathrm{q})\begin{pmatrix}1\\0\end{pmatrix} = \begin{pmatrix} b + p\sin^2\beta \\ -p\sin\beta\cos\beta \end{pmatrix} \text{ and}$$
$$(\mathrm{q})\begin{pmatrix}0\\1\end{pmatrix} = \begin{pmatrix} -p\sin\beta\cos\beta \\ b - p\sin^2\beta \end{pmatrix}$$

show clearly that the diagonal and the nondiagonal elements of the matrix (q) are, respectively, the spin-flip and the non-spin-flip scattering lengths. It is usual to consider the scattering cross sections, which are the measurable quantities. The cross sections for neutrons polarized parallel or antiparallel to the ion magnetic moment are

$$(\mathrm{d}\sigma/\mathrm{d}\Omega)_{\pm} = b^2 \pm 2bp\sin^2\beta + (p\sin\beta)^2. \qquad (5.3.3.7)$$

These expressions are the sum of the spin-flip and non-spin-flip cross sections, which are equal to $(b \pm p\sin^2\beta)^2$ and $(p\sin\beta\cos\beta)^2$, respectively. In the case of nonpolarized neutrons, the interference term $(\pm 2bp\sin^2\beta)$ between the nuclear and the magnetic scattering disappears; the cross section is then

$$(\mathrm{d}\sigma/\mathrm{d}\Omega) = b^2 + (p\sin\beta)^2. \qquad (5.3.3.8)$$

In the general case of a partially polarized beam we can use the density-matrix representation. Let ρ_{inc} be the density matrix of the incident beam; it can be shown that the density matrix of the diffracted beam is equal to the following product of matrices: $(\mathrm{q})\rho_{inc}(\mathrm{q}^*)$. Using the relations between the density matrix and polarization vector presented in the preceding section, we can obtain a general description of the diffracted beam as a function of the polarization properties of the incident beam. Such a formalism is of interest for dealing with new experimental arrangements, in which a three-dimensional polarization analysis of the diffracted beam is possible, as shown by Tasset (1989).

5.3.3.3. Dynamical theory in the case of perfect ferromagnetic or collinear ferrimagnetic crystals

The most direct way to develop this dynamical theory in the two-beam case, which involves a single Bragg-diffracted beam of diffraction vector $\mathbf{h}$, is to consider spinor wavefunctions of the following form:

$$\varphi(\mathbf{r}) = \exp(i\mathbf{K_0}\cdot\mathbf{r})\begin{pmatrix}D_0\\E_0\end{pmatrix} + \exp[i(\mathbf{K_0}+\mathbf{h})\mathbf{r}]\begin{pmatrix}D_h\\E_h\end{pmatrix} \qquad (5.3.3.9)$$

as approximate solutions of the wave equation inside the crystal,

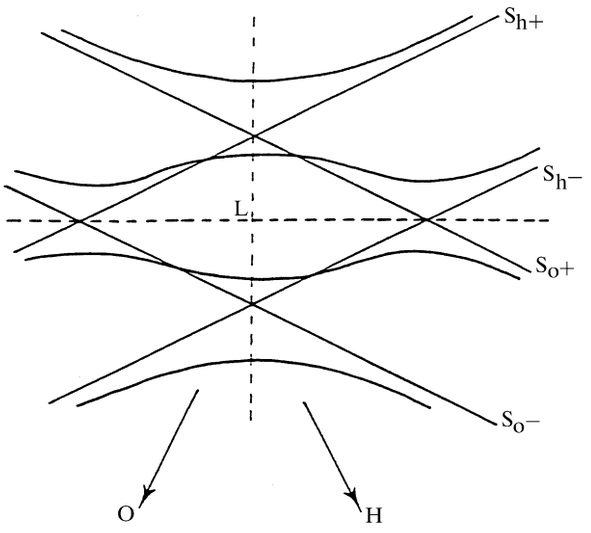

Fig. 5.3.3.1. Schematic plot of the two-beam dispersion surface in the case of a purely magnetic reflection such that $\mathbf{Q_h} = \mathbf{Q_{-h}} = \mathbf{Q_0}$ and that the angle between $\mathbf{Q_0}$ and $\mathbf{Q_h}$ is equal to $\pi/4$.

$$\Delta\varphi(\mathbf{r}) + k^2\varphi(\mathbf{r}) = [u(\mathbf{r}) - \boldsymbol{\sigma}\cdot\mathbf{Q}(\mathbf{r})]\varphi(\mathbf{r}), \qquad (5.3.3.10)$$

where $u(\mathbf{r})$ and $-\boldsymbol{\sigma}\cdot\mathbf{Q}(\mathbf{r})$ are, respectively, equal to the nuclear and the magnetic potential energies multiplied by $2m/\hbar^2$. In the calculation of $\varphi(\mathbf{r})$ in the two-beam case, we need only three terms in the expansions of the functions $u(\mathbf{r})$ and $\mathbf{Q}(\mathbf{r})$ into Fourier series:

$$u(\mathbf{r}) = u_0 + u_{\mathbf{h}}\exp(i\mathbf{h}\cdot\mathbf{r}) + u_{-\mathbf{h}}\exp(-i\mathbf{h}\cdot\mathbf{r}) + \ldots,$$
$$\mathbf{Q}(\mathbf{r}) = \mathbf{Q_0} + \mathbf{Q_h}\exp(i\mathbf{h}\cdot\mathbf{r}) + \mathbf{Q_{-h}}\exp(-i\mathbf{h}\cdot\mathbf{r}) + \ldots.$$

We suppose that the crystal is magnetically saturated by an externally applied magnetic field $\mathbf{H}_a$. $\mathbf{Q_0}$ is then proportional to the macroscopic mean magnetic field $\mathbf{B} = \mu_0(\mathbf{M} + \mathbf{H}_a + \mathbf{H}_d)$, where $\mathbf{M}$ is the magnetization vector and $\mathbf{H}_d$ is the demagnetizing field. The results of Section 5.3.3.2 show that $\mathbf{Q_h}$ and $\mathbf{Q_{-h}}$ are proportional to the projection of $\mathbf{M}$ on the reflecting plane.

The four coefficients D_0, D_h, E_0 and E_h of (5.3.3.9) are found to satisfy a system of four homogeneous linear equations. The condition that the associated determinant has to be equal to 0 defines the dispersion surface, which is of order 4 and has four branches. An incident plane wave thus excites a system of four wavefields of the form of (5.3.3.9), generally polarized in various directions. A particular example of a dispersion surface, having an unusual shape, is shown in Fig. 5.3.3.1.

This is a much more complicated situation than in the case of nonmagnetic crystals, in which one only needs to consider scalar wavefunctions which depend on two coefficients, such as D_0 and D_h, and which are related to hyperbolic dispersion surfaces of order 2, as fully described in Chapter 5.1 on X-ray diffraction.

In fact, all neutron experiments related to dynamical effects in diffraction by magnetic crystals have been performed under such conditions that the magnetization vector in the crystal is perpendicular to the diffraction vector $\mathbf{h}$. In this case, the vectors $\mathbf{Q_h}$ and $\mathbf{Q_{-h}}$ are parallel or antiparallel to the vector $\mathbf{Q_0}$ which is chosen as the spin-quantization axis. The matrices $\boldsymbol{\sigma}\cdot\mathbf{Q_0}$, $\boldsymbol{\sigma}\cdot\mathbf{Q_h}$ and $\boldsymbol{\sigma}\cdot\mathbf{Q_{-h}}$ are then all diagonal matrices, and we obtain for the two spin states $(\pm)$ separate dynamical equations which are similar to the dynamical equations for the scalar case, but with different structure factors, which are either the sum or the difference of the nuclear structure factor F_N and of the magnetic structure factor F_M:

$$F_+ = F_N + F_M \text{ and } F_- = F_N - F_M. \quad (5.3.3.11)$$

F_N and F_M are related to the scattering lengths of the ions in the unit cell of volume V_c:

$$F_N = V_c u_{\mathbf{h}} = \sum_i b_i \exp(-i\mathbf{h}\cdot\mathbf{r}_i);$$

$$F_M = V_c|\mathbf{Q}_{\mathbf{h}}| = -\frac{\mu_0 m}{2h^2}\mu_n \boldsymbol{\sigma}\cdot\sum_i \boldsymbol{\mu}_{i\perp}(\mathbf{h}) f_i\left(\frac{\sin\theta}{\lambda}\right)\exp(-i\mathbf{h}\cdot\mathbf{r}_i).$$

The dispersion surface of order 4 degenerates into two hyperbolic dispersion surfaces, each of them corresponding to one of the polarization states (±). The asymptotes are different; this is related to different values of the refractive indices for neutron polarization parallel or antiparallel to $\mathbf{Q}_0$.

In some special cases the magnitudes of F_N and F_M happen to be equal. Only one polarization state is then reflected. Magnetic crystals with such a property (reflections 111 of the Heusler alloy Cu_2MnAl, or 200 of the alloy Co–8% Fe) are very useful as polarizing monochromators and as analysers of polarization.

If the scattering vector $\mathbf{h}$ is in the same direction as the magnetization, this reflection is a purely nuclear one (with no magnetic contribution), since F_M is then equal to 0. Purely magnetic reflections (without nuclear contribution) also exist if the magnetic structure involves several sublattices.

If $\mathbf{h}$ is neither perpendicular to the average magnetization nor in the same direction, the presence of nondiagonal matrices in the dynamical equations cannot be avoided. The dynamical theory of diffraction by perfect magnetic crystals then takes the complicated form already mentioned.

Theoretical discussions of this complicated case of dynamical diffraction have been given by Stassis & Oberteuffer (1974), Mendiratta & Blume (1976), Sivardière (1975), Belyakov & Bokun (1975, 1976), Schmidt *et al.* (1975), Bokun (1979), Guigay & Schlenker (1979*a*,*b*) and Schmidt (1983). However, to our knowledge, only limited experimental work has been carried out on this subject. Successful experiments could only be performed for the simpler cases mentioned above.

5.3.3.4. The dynamical theory in the case of perfect collinear antiferromagnetic crystals

In this case, there is no average magnetization ($\mathbf{Q}_0 = 0$). It is then convenient to choose the quantization axis in the direction of $\mathbf{Q}_{\mathbf{h}}$ and $\mathbf{Q}_{-\mathbf{h}}$. The dispersion surface degenerates into two hyperbolic surfaces corresponding to each polarization state along this direction for any orientation of the diffraction vector relative to the direction of the magnetic moments of the sublattices. These two hyperbolic dispersion surfaces have the same asymptotes. Furthermore, in the case of a purely magnetic reflection, they are identical.

The possibility of observing a precession of the neutron polarization in the presence of diffraction, in spite of the fact that there is no average magnetization, has been pointed out by Baryshevskii (1976).

5.3.3.5. The flipping ratio

In polarized neutron diffraction by a magnetically saturated magnetic sample, it is usual to measure the ratio of the reflected intensities I_+ and I_- measured when the incident beam is polarized parallel or antiparallel to the magnetization in the sample. This ratio is called the flipping ratio,

$$R = I_+/I_-, \quad (5.3.3.12)$$

because its measurement involves flipping the incident-beam polarization to the opposite direction. This is an experimentally well defined quantity, because it is independent of a number of parameters such as the intensity of the incident beam, the temperature factor or the coefficient of absorption. In the case of an ideally imperfect crystal, we obtain from the kinematical expressions of the integrated reflectivities

$$R_{\text{kin}}(\mathbf{h}) = (I_+/I_-)_{\text{kin}} = \left(\frac{|F_N + F_M|}{|F_N - F_M|}\right)^2. \quad (5.3.3.13)$$

In the case of an ideally perfect thick crystal, we obtain from the dynamical expressions of the integrated reflectivities

$$R_{\text{dyn}}(\mathbf{h}) = (I_+/I_-)_{\text{dyn}} = \frac{|F_N + F_M|}{|F_N - F_M|}. \quad (5.3.3.14)$$

In general, R_{dyn} depends on the wavelength and on the crystal thickness; these dependences disappear, as seen from (5.3.3.14), if the path length in the crystal is much larger than the extinction distances for the two polarization states. It is clear that the determination of R_{kin} or R_{dyn} allows the determination of the ratio F_M/F_N, hence of F_M if F_N is known. In fact, because real crystals are neither ideally imperfect nor ideally perfect, one usually introduces an extinction factor y (extinction is discussed below, in Section 5.3.4) in order to distinguish the real crystal reflectivity from the reflectivity of the ideally imperfect crystal. Different extinction coefficients y_+ and y_- are actually expected for the two polarization states. This obviously complicates the task of the determination of F_M/F_N.

In the kinematical approximation, the flipping ratio does not depend on the wavelength, in contrast to dynamical calculations for hypothetically perfect crystals (especially for the Laue case of diffraction). Therefore, an experimental investigation of the wavelength dependence of the flipping ratio is a convenient test for the presence of extinction. Measurements of the flipping ratio have been used by Bonnet *et al.* (1976) and by Kulda *et al.* (1991) in order to test extinction models. Baruchel *et al.* (1986) have compared nuclear and magnetic extinction in a crystal of MnP.

Instead of considering only the ratio of the integrated reflectivities, it is also possible to record the flipping ratio as a function of the angular position of the crystal as it is rotated across the Bragg position. Extinction is expected to be maximum at the peak and the ratio measured on the tails of the rocking curve may approach the kinematical value. It has been found experimentally that this expectation is not of general validity, as discussed by Chakravarthy & Madhav Rao (1980). It would be valid in the case of a perfect crystal, hence in the case of pure primary extinction. It would also be valid in the case of secondary extinction of type I, but not in the case of secondary extinction of type II [following Zachariasen (1967), type II corresponds to mosaic crystals such that the diffraction pattern from each block is wider than the mosaic statistical distribution].

5.3.4. Extinction in neutron diffraction (nonmagnetic case)

The kinematical approximation, which corresponds to the first Born approximation in scattering theory, supposes that each incident neutron can be scattered only once and therefore neglects the possibility that the neutrons may be scattered several times. Because this is a simple approximation which overestimates the crystal reflectivity, the actual reduction of reflectivity, as compared to its kinematical value, is termed *extinction.* This is actually a typical dynamical effect, since it is a multiple-scattering effect.

Extinction effects can be safely neglected in the case of scattering by very small crystals; more precisely, this is possible when the path length of the neutron beam in the crystal is much smaller than $\Delta = V_c/\lambda F$, where λ is the neutron wavelength and F/V_c is the scattering length per unit volume for the reflection considered. Δ is sometimes called the 'extinction distance'.

A very important fact is that extinction effects also vanish if the crystal is imperfect enough, because each plane-wave component of the incident beam can then be Bragg-reflected in only a small volume of the sample. This is the extinction-free case of 'ideally imperfect crystals'. Conversely, extinction is maximum (smallest value of y) in the case of ideally perfect non-absorbing crystals.

Clearly, no significant extinction effects are expected if the crystal is thick but strongly absorbing, more precisely if the linear absorption coefficient μ is such that $\mu\Delta \gg 1$. Neutron diffraction usually corresponds to the opposite case ($\mu\Delta \ll 1$), in which extinction effects in nearly perfect crystals dominate absorption effects.

Extinction effects are usually described in the frame of the mosaic model, in which the crystal is considered as a juxtaposition of perfect blocks with different orientations. The relevance of this model to the case of neutron diffraction was first considered by Bacon & Lowde (1948). If the mosaic blocks are big enough there is extinction within each block; this is called *primary extinction.* Multiple scattering can also occur in different blocks if their misorientation is small enough. In this case, which is called *secondary extinction*, there is no phase coherence between the scattering events in the different blocks. The fact that empirical intensity-coupling equations are used in this case is based on this phase incoherence.

In the general case, primary and secondary extinction effects coexist. Pure secondary extinction occurs in the case of a mosaic crystal made of very small blocks. Pure primary extinction is observed in diffraction by perfect crystals.

The parameters of the mosaic model are the average size of the perfect blocks and the angular width of their misorientation distribution. The extinction theory of the mosaic model provides a relation between these parameters and the extinction coefficient, defined as the ratio of the observed reflectivity to the ideal one, which is the kinematical reflectivity in this context.

In conventional work, the crystal structure factors of different reflections and the parameters of the mosaic model are fitted together to the experimental data, which are the integrated reflectivities and the angular widths of the rocking curves. In many cases, only the weakest reflections will be free, or nearly free, from extinction. The extinction corrections thus obtained can be considered as satisfactory in cases of moderate extinction. Nevertheless, extinction remains a real problem in cases of strong extinction and in any case if a very precise determination of the crystal structure factors is required.

There exist several forms of the mosaic model of extinction. For instance, in the model developed by Kulda (1988*a*,*b*, 1991), the mosaic blocks are not considered just as simple perfect blocks but may be deformed perfect blocks. This has the advantage of including the case of macroscopically deformed crystals, such as bent crystals.

A basically different approach, free from the distinction between primary and secondary extinction, has been proposed by Kato (1980*a*,*b*). This is a wave-optical approach starting from the dynamical equations for diffraction by deformed crystals. These so-called Takagi–Taupin equations (Takagi, 1962; Taupin, 1964) contain a position-dependent phase factor related to the displacement field of the deformed crystal lattice. Kato proposed considering this phase factor as a random function with suitably defined statistical characteristics. The wave amplitudes are then also random functions, the average of which represent the coherent wavefields while their statistical fluctuations represent the incoherent intensity fields.

Modifications to the Kato formulation have been introduced by Al Haddad & Becker (1988), by Becker & Al Haddad (1990, 1992), by Guigay (1989) and by Guigay & Chukhovskii (1992, 1995). Presently, it is not easy to apply this 'statistical dynamical theory' to real experiments. The widely used methods for extinction corrections are still based on the former mosaic model, according to the formulation of Zachariasen (1967), later improved by Becker & Coppens (1974*a*,*b*, 1975).

As in the X-ray case, acoustic waves produced by ultrasonic excitation can artificially induce a transition from perfect to ideally imperfect crystal behaviour. The effect of ultrasound on the scattering behaviour of distorted crystals is quite complex. A good discussion with reference to neutron-scattering experiments is given by Zolotoyabko & Sander (1995).

The situation of crystals with a simple distortion field is less difficult than the statistical problem of extinction. Klar & Rustichelli (1973) confirmed that the Takagi–Taupin equations, originally devised for X-rays, can be used for neutron diffraction with due account of the very small absorption, and used them for computing the effect of crystal curvature.

5.3.5. Effect of external fields on neutron scattering by perfect crystals

The possibility of acting on neutrons through externally applied fields during their propagation in perfect crystals provides possibilities that are totally unknown in the X-ray case. The theory has been given by Werner (1980) using the approaches (migration of tie points, and Takagi–Taupin equations) that are customary in the treatment of imperfect crystals (see above). Zeilinger *et al.* (1986) pointed out that the effective-mass concept, familiar in describing electrons in solid-state physics, can shed new light on this behaviour: because of the curvature of the dispersion surface at a near-exact Bragg setting, effective masses five orders of magnitude smaller than the rest mass of the neutron in a vacuum can be obtained. Related experiments are discussed below.

An interesting proposal was put forward by Horne *et al.* (1988) on the coupling between the Larmor precession in a homogeneous magnetic field and the spin–orbit interaction of the neutron with nonmagnetic atoms, a term which was dismissed in Section 5.3.2 because its contribution to the scattering length is two orders of magnitude smaller than that of the nuclear term. A resonance is expected to show up as highly enhanced diffracted intensity when a perfect sample is set for Bragg scattering and the magnetic field is adjusted so that the Larmor precession period is equal to the *Pendellösung* period.

5.3.6. Experimental tests of the dynamical theory of neutron scattering

These experiments are less extensive for neutron scattering than for X-rays. The two most striking effects of dynamical theory for nonmagnetic nearly perfect crystals, *Pendellösung* behaviour and anomalous absorption, have been demonstrated in the neutron case too. *Pendellösung* measurement is described below (Section 5.3.7.2) because it is useful in the determination of scattering lengths. The anomalous transmission effect occurring when a perfect absorbing crystal is exactly at Bragg setting, *i.e.* the Borrmann effect, is often referred to in the neutron case as the suppression of the inelastic channel in resonance scattering, after Kagan & Afanas'ev (1966), who worked out the theory. A small decrease in absorption was detected in pioneering experiments on calcite by Knowles (1956) using the corresponding decrease in the emission of γ-rays and by Sippel *et al.* (1962), Shil'shtein *et al.* (1971) and Hastings *et al.* (1990) directly. Rocking curves of perfect crystals were measured by Sippel *et al.* (1964) in transmission, and by Kikuta *et al.* (1975). Integrated intensities were

measured by Lambert & Malgrange (1982). The large angular amplification associated with the curvature of the dispersion surfaces near the exact Bragg setting was demonstrated by Kikuta *et al.* (1975) and by Zeilinger & Shull (1979).

In magnetic crystals, the investigations have been restricted to the simpler geometry where the scattering vector is perpendicular to the magnetization, and to few materials. *Pendellösung* behaviour was evidenced through the variation with wavelength of the flipping ratio for polarized neutrons by Baruchel *et al.* (1982) on an yttrium iron garnet sample, with the geometry selected so that the defects would not affect the Bragg reflection used. The inclination method was used successfully by Zelepukhin *et al.* (1989), Kvardakov & Somenkov (1990) and Kvardakov *et al.* (1990*a*) for the weak ferromagnet $FeBO_3$, and in the room-temperature weak-ferromagnetic phase of hematite, α-Fe_2O_3, by Kvardakov *et al.* (1990*b*) and Kvardakov & Somenkov (1992).

Experiments on the influence of defects in nearly perfect crystals have been performed by several groups. The effect on the rocking curve was investigated by Eichhorn *et al.* (1967), the intensities were measured by Lambert & Malgrange (1982) and by Albertini, Boeuf, Cesini *et al.* (1976), and the influence on the *Pendellösung* behaviour was discussed by Kvardakov & Somenkov (1992). Boeuf & Rustichelli (1974) and Albertini *et al.* (1977) investigated silicon crystals curved by a thin surface silicon nitride layer.

Many experiments have been performed on vibrating crystals; reviews are given by Michalec *et al.* (1988) and by Kulda *et al.* (1988). Because the velocity of neutrons is of the same order of magnitude as the velocity of acoustic phonons in crystals, the effect of ultrasonic excitation on dynamical diffraction takes on some original features compared to the X-ray case (Iolin & Entin, 1983); they could to some extent be evidenced experimentally (Iolin *et al.*, 1986; Chalupa *et al.*, 1986). References to experimental work on neutron scattering by imperfect crystals under ultrasonic excitation are included in Zolotoyabko & Sander (1995).

Some experiments with no equivalent in the X-ray case could be performed. The very strong incoherent scattering of neutrons by protons, very different physically but similar in its effect to absorption, was also shown to lead to anomalous transmission effects by Sippel & Eichhorn (1968). Because the velocity of thermal neutrons in a vacuum is five orders of magnitude smaller than the velocity of light, the flight time for neutrons undergoing Bragg scattering in Laue geometry in a perfect crystal could be measured directly (Shull *et al.*, 1980). The effect of externally applied fields was measured experimentally for magnetic fields by Zeilinger & Shull (1979) and Zeilinger *et al.* (1986). Slight rotation of the crystal, introducing a Coriolis force, was used by Raum *et al.* (1995), and gravity was tested recently, with the spectacular result that some states are accelerated upwards (Zeilinger, 1995).

5.3.7. Applications of the dynamical theory of neutron scattering

5.3.7.1. Neutron optics

Most experiments in neutron scattering require an intensity-effective use of the available beam at the cost of relatively high divergence and wavelength spread. The monochromators must then be imperfect ('mosaic') crystals. In some cases, however, it is important to have a small divergence and wavelength band. One example is the search for small variations in neutron energy in inelastic scattering without the use of the neutron spin-echo principle. Perfect crystals must then be used as monochromators or analysers, and dynamical diffraction is directly involved. As in the X-ray case, special designs can lead to strong decrease in the intensity of harmonics, *i.e.* of contributions of $\lambda/2$ or $\lambda/3$ (Hart & Rodrigues, 1978). The possibility of focusing neutron beams by the use of perfect crystals with the incident beam spatially modulated in amplitude through an absorber, or in phase through an appropriate patterning of the surface, in analogy with the Bragg–Fresnel lenses developed for X-rays, was suggested by Indenbom (1979).

The use of two identical perfect crystals in nondispersive (+, −, ‖) setting provides a way of measuring the very narrow intrinsic rocking curves expected from the dynamical theory. Any divergence added between the two crystals can be sensitively measured. Thus perfect crystals provide interesting possibilities for measuring very small angle neutron scattering. This was performed by Takahashi *et al.* (1981, 1983) and Tomimitsu *et al.* (1986) on amorphous materials, and by Kvardakov *et al.* (1987) for the investigation of ferromagnetic domains in bulk silicon–iron specimens under stress, both through the variations in transmission associated with refraction on the domain walls and through small-angle scattering. Imaging applications are described in Section 5.3.7.4. Badurek *et al.* (1979) used the different deflection of the two polarization states provided by a magnetic prism placed between two perfect silicon crystals to produce polarized beams.

Curved almost-perfect crystals or crystals with a gradient in the lattice spacing can provide focusing (Albertini, Boeuf, Lagomarsino *et al.*, 1976) and vibrating crystals can give the possibility of tailoring the reflectivity of crystals, as well as of modulating beams in time (Michalec *et al.*, 1988). A double-crystal arrangement with bent crystals was shown by Eichhorn (1988) to be a flexible small-angle-neutron-scattering device.

5.3.7.2. Measurement of scattering lengths by Pendellösung effects

As in X-ray diffraction, *Pendellösung* oscillations provide an accurate way of measuring structure factors, hence coherent neutron scattering lengths. The equal-thickness fringes expected from a wedge-shaped crystal were observed by Kikuta *et al.* (1971). Three kinds of measurements were made. Sippel *et al.* (1965) measured as a function of thickness the integrated reflectivity from a perfect crystal of silicon, the thickness of which they varied by polishing after each measurement, obtaining a curve similar to Fig. 5.1.6.7, corresponding to equation 5.1.6.8. Shull (1968) restricted the measurement to wavefields that propagated along the reflecting planes, hence at exact Bragg incidence, by setting fine slits on the entrance and exit faces of 3 to 10 mm-thick silicon crystals, and measured the oscillation in diffracted intensity as he varied the wavelength of the neutrons used by rotating the crystal. Shull & Oberteuffer (1972) showed that a better interpretation of the data, when the beam is restricted to a fine slit, corresponds to the spherical wave approach (actually cylindrical wave), and the boundary conditions were discussed more generally by Arthur & Horne (1985). Somenkov *et al.* (1978) developed the inclination method, in which the integrated reflectivity is measured as the effective crystal thickness is varied nondestructively, by rotating the crystal around the diffraction vector, and used it for germanium. Belova *et al.* (1983) discuss this method in detail. The results obtained by this group for magnetic crystals are mentioned in Section 5.3.6. Structure-factor values for magnetic reflections were obtained by Kvardakov *et al.* (1995) for the weak ferromagnet $FeBO_3$.

5.3.7.3. Neutron interferometry

Because diffraction by perfect crystals provides a well defined distribution of the intensity and phase of the beam, interferometry with X-rays or neutrons is possible using ingeniously designed and carefully manufactured monolithic devices carved out of single crystals of silicon. The technical and scientific features of this family of techniques are well summarized by Bonse (1979, 1988), as well as other papers in the same volumes, and by Shull (1986).

X-ray interferometry started with the Bonse–Hart interferometer (Bonse & Hart, 1965). A typical device is the LLL skew-symmetric interferometer, where the L's stand for Laue,

indicating transmission geometry in all crystal slabs. In these slabs, which can be called the splitter, the mirrors and the recombiner, the same pair of opposite reflections, in symmetrical Laue geometry, is used three times. In the first slab, the incident beam is coherently split into a transmitted and a diffracted beam. Each of these is then diffracted in the two mirrors, and the resulting beams interfere in the recombiner, again yielding a forward-diffracted and a diffracted beam, the intensities of both of which are measured. This version, the analogue of the Mach–Zehnder interferometer in optics, offers a sizeable space (several cm of path length) where two coherent parallel beams can be submitted to various external actions. Shifting the relative phase of these beams (*e.g.* by π, introducing an optical path-length difference of $\lambda/2$) results in the intensities of the outgoing beams changing from a maximum to a minimum.

Applications of neutron interferometry range from the very useful to the very exotic. The most useful one is probably the measurement of coherent neutron scattering lengths. Unlike the *Pendellösung* method described in Section 5.3.7.2, this method does not require the measured samples to be perfect single crystals, nor indeed crystals. Placing a slab of material across one of the beams and rotating it will induce an optical path-length difference of $(1 - n)t$ if t is the effective thickness along the beam, hence a phase shift of $2\pi(1 - n)t/\lambda$. With the expression of the refractive index n as given in Section 5.3.2.2, it is clear that for an isotopically pure material the scattering length $b_{\rm coh}$ can be deduced from the measurement of intensity *versus* the rotation angle of the phase shifter. This is a very versatile and much used method. The decrease in oscillation contrast can be used to obtain information of relevance to materials science, such as statistical properties of magnetic domain distributions (Korpiun, 1966) or precipitates (Rauch & Seidl, 1987); Rauch (1995) analyses the effect in terms of the neutron coherence function.

Many elegant experiments have been performed with neutron interferometers in efforts to set an upper limit to effects than can be considered as nonexistent, or to test expectations of basic quantum physics. Many papers are found in the same volumes as Bonse (1979) and Bonse (1988); excellent reviews have been given by Klein & Werner (1983), Klein (1988) and Werner (1995). Among the topics investigated are the effect of gravity (Colella *et al.*, 1975), the Sagnac effect, *i.e.* the influence of the Earth's rotation (Werner *et al.*, 1979), the Fizeau effect, *i.e.* the effect of the movement of the material through which the neutrons are transmitted (Arif *et al.*, 1988) and the Aharonov–Casher effect, *i.e.* the dual of the Aharonov–Bohm effect for neutral particles having a magnetic moment (Cimmino *et al.*, 1989).

5.3.7.4. Neutron diffraction topography and other imaging methods

These are the neutron form of the 'topographic' or diffraction imaging techniques, in which an image of a single crystal is obtained through the local variations in Bragg-diffracted intensity due to inhomogeneities in the sample. It is briefly described in Chapter 2.8 of *IT* C. It was pioneered by Doi *et al.* (1971) and by Ando & Hosoya (1972). Like its X-ray counterpart, neutron topography can reveal isolated defects, such as dislocations (Schlenker *et al.*, 1974; Malgrange *et al.*, 1976). Because of the small neutron fluxes available, it is not very convenient for this purpose, since the resolution is poor or the exposure times are very long. On the other hand, the very low absorption of neutrons in most materials makes it quite convenient for observing the gross defect structure in samples that would be too absorbing for X-rays (Tomimitsu & Doi, 1974; Baruchel *et al.*, 1978; Tomimitsu *et al.*, 1983; Kvardakov *et al.*, 1992), or the spatial modulation of distortion due to vibration, for example in quartz (Michalec *et al.*, 1975), and resonant magnetoelastic effects (Kvardakov & Somenkov, 1991). In particular, virtual slices of bulky as-grown samples can be investigated without cutting them using neutron section topography or neutron tomography (Schlenker *et al.*, 1975; Davidson & Case, 1976).

Neutron topography also shows the salient dynamical interference effect, *viz Pendellösung*, visually, in the form of fringes (Kikuta *et al.*, 1971; Malgrange *et al.*, 1976; Tomimitsu & Zeyen, 1978). Its unique feature, however, is the possibility of observing and directly characterizing inhomogeneities in the magnetic structure, *i.e.* magnetic domains of all kinds [ferromagnetic domains (Schlenker & Shull, 1973) and antiferromagnetic domains of various sorts (Schlenker & Baruchel, 1978), including spin-density wave domains (Ando & Hosoya, 1972, 1978; Davidson *et al.*, 1974), 180° or time-reversed domains in some materials and helimagnetic or chirality domains (Baruchel *et al.*, 1990)], or coexisting phases at a first-order phase transition (Baruchel, 1989). In such cases, the contrast is primarily due to local variations in the structure factor, a situation very unusual in X-ray topography, and good crystal quality, leading to dynamical scattering behaviour, is essential in the observation process only in a few cases (Schlenker *et al.*, 1978). It is often crucial, however, for making the domain structure simple enough to be resolved, in particular in the case of antiferromagnetic domains.

Imaging can also be performed for samples that need be neither crystals nor perfect. Phase-contrast imaging of a specimen through which the neutrons are transmitted can be performed in a neutron interferometer. It has been shown to reveal thickness variations by Bauspiess *et al.* (1978) and ferromagnetic domains by Schlenker *et al.* (1980). The same papers showed that phase edges show up as contrast when one of the interferometer paths is blocked, *i.e.* when the sample is placed effectively between perfect, identical crystals set for diffraction in a nondispersive setting. Under the name of neutron radiography with refraction contrast, this technique, essentially a form of Schlieren imaging, was further developed by Podurets, Somenkov & Shil'shtein (1989), Podurets, Somenkov, Chistyakov & Shil'shtein (1989), and Podurets *et al.* (1991), who were able to image internal ferromagnetic domain walls in samples 10 mm thick.

References

Albertini, G., Boeuf, A., Cesini, G., Mazkedian, S., Melone, S. & Rustichelli, F. (1976). *A simple model for dynamical neutron diffraction by deformed crystals. Acta Cryst.* A**32**, 863–868.

Albertini, G., Boeuf, A., Klar, B., Lagomarsino, S., Mazkedian, S., Melone, S., Puliti, P. & Rustichelli, F. (1977). *Dynamical neutron diffraction by curved crystals in the Laue geometry. Phys. Status Solidi A*, **44**, 127–136.

Albertini, G., Boeuf, A., Lagomarsino, S., Mazkedian, S., Melone, S. & Rustichelli, F. (1976). *Neutron properties of curved monochromators. Proceedings of the Conference on Neutron Scattering, Gatlinburg, Tennessee*, USERDA CONF 760601-P2, 1151–1158. Oak Ridge, Tennessee: Oak Ridge National Laboratory.

Al Haddad, M. & Becker, P. J. (1988). *On the statistical dynamical theory of diffraction: application to silicon. Acta Cryst.* A**44**, 262–270.

Ando, M. & Hosoya, S. (1972). *Q-switch and polarization domains in antiferromagnetic chromium observed with neutron-diffraction topography. Phys. Rev. Lett.* **29**, 281–285.

Ando, M. & Hosoya, S. (1978). *Size and behavior of antiferromagnetic domains in Cr directly observed with X-ray and neutron topography. J. Appl. Phys.* **49**, 6045–6051.

Arif, M., Kaiser, H., Clothier, R., Werner, S. A., Berliner, R., Hamilton, W. A., Cimmino, A. & Klein, A. G. (1988). *Fizeau effect for neutrons passing through matter at a nuclear resonance. Physica B*, **151**, 63–67.

Arthur, J. & Horne, M. A. (1985). *Boundary conditions in dynamical neutron diffraction. Phys. Rev. B*, **32**, 5747–5752.

Bacon, G. E. & Lowde, R. D. (1948). *Secondary extinction and neutron crystallography. Acta Cryst.* **1**, 303–314.

Badurek, G., Rauch, H., Wilfing, A., Bonse, U. & Graeff, W. (1979). *A perfect-crystal neutron polarizer as an application of magnetic prism refraction. J. Appl. Cryst.* **12**, 186–191.

Baruchel, J. (1989). *The contribution of neutron and synchrotron radiation topography to the investigation of first-order magnetic phase transitions. Phase Transit.* **14**, 21–29.

Baruchel, J., Guigay, J. P., Mazuré-Espejo, C., Schlenker, M. & Schweizer, J. (1982). *Observation of Pendellösung effect in polarized neutron scattering from a magnetic crystal. J. Phys.* **43**, C7, 101–106.

Baruchel, J., Patterson, C. & Guigay, J. P. (1986). *Neutron diffraction investigation of the nuclear and magnetic extinction in MnP. Acta Cryst.* A**42**, 47–55.

Baruchel, J., Schlenker, M. & Palmer, S. B. (1990). *Neutron diffraction topographic investigations of "exotic" magnetic domains. Nondestruct. Test. Eval.* **5**, 349–367.

Baruchel, J., Schlenker, M., Zarka, A. & Pétroff, J. F. (1978). *Neutron diffraction topographic investigation of growth defects in natural lead carbonate single crystals. J. Cryst. Growth*, **44**, 356–362.

Baryshevskii, V. G. (1976). *Particle spin precession in antiferromagnets. Sov. Phys. Solid State*, **18**, 204–208.

Bauspiess, W., Bonse, U., Graeff, W., Schlenker, M. & Rauch, H. (1978). Result shown in Bonse (1979).

Becker, P. & Al Haddad, M. (1990). *Diffraction by a randomly distorted crystal. I. The case of short-range order. Acta Cryst.* A**46**, 123–129.

Becker, P. & Al Haddad, M. (1992). *Diffraction by a randomly distorted crystal. II. General theory. Acta Cryst.* A**48**, 121–134.

Becker, P. J. & Coppens, P. (1974*a*). *Extinction within the limit of validity of the Darwin transfer equations. I. General formalisms for primary and secondary extinction and their application to spherical crystals. Acta Cryst.* A**30**, 129–147.

Becker, P. J. & Coppens, P. (1974*b*). *Extinction within the limit of validity of the Darwin transfer equations. II. Refinement of extinction in spherical crystals of SrF_2 and LiF. Acta Cryst.* A**30**, 148–153.

Becker, P. J. & Coppens, P. (1975). *Extinction within the limit of validity of the Darwin transfer equations. III. Non-spherical crystals and anisotropy of extinction. Acta Cryst.* A**31**, 417–425.

Belova, N. E., Eichhorn, F., Somenkov, V. A., Utemisov, K. & Shil'shtein, S. Sh. (1983). *Analyse der Neigungsmethode zur Untersuchung von Pendellösungsinterferenzen von Neutronen und Röntgenstrahlen. Phys. Status Solidi A*, **76**, 257–265.

Belyakov, V. A. & Bokun, R. Ch. (1975). *Dynamical theory of neutron diffraction by perfect antiferromagnetic crystals. Sov. Phys. Solid State*, **17**, 1142–1145.

Belyakov, V. A. & Bokun, R. Ch. (1976). *Dynamical theory of neutron diffraction in magnetic crystals. Sov. Phys. Solid State*, **18**, 1399–1402.

Boeuf, A. & Rustichelli, F. (1974). *Some neutron diffraction experiments on curved silicon crystals. Acta Cryst.* A**30**, 798–805.

Bokun, R. Ch. (1979). *Beats in the integrated intensity in neutron diffraction by perfect magnetic crystals. Sov. Phys. Tech. Phys.* **24**, 723–724.

Bonnet, M., Delapalme, A., Becker, P. & Fuess, H. (1976). *Polarised neutron diffraction – a tool for testing extinction models: application to yttrium iron garnet. Acta Cryst.* A**32**, 945–953.

Bonse, U. (1979). *Principles and methods of neutron interferometry*. In *Neutron Interferometry: Proceedings of an International Workshop*, edited by U. Bonse & H. Rauch, pp. 3–33. Oxford: Clarendon Press.

Bonse, U. (1988). *Recent advances in X-ray and neutron interferometry. Physica B*, **151**, 7–21.

Bonse, U. & Hart, M. (1965). *An X-ray interferometer. Appl. Phys. Lett.* **6**, 155–156.

Chakravarthy, R. & Madhav Rao, L. (1980). *A simple method to correct for secondary extinction in polarised-neutron diffractometry. Acta Cryst.* A**36**, 139–142.

Chalupa, B., Michalec, R., Horalik, L. & Mikula, P. (1986). *The study of neutron acoustic effect by neutron diffraction on InSb single crystal. Phys. Status Solidi A*, **97**, 403–409.

Cimmino, A., Opat, G. I., Klein, A. G., Kaiser, H., Werner, S. A., Arif, M. & Clothier, R. (1989). *Observation of the topological Aharonov–Casher phase shift by neutron interferometry. Phys. Rev. Lett.* **63**, 380–383.

Colella, R., Overhauser, A. W. & Werner, S. A. (1975). *Observation of gravitationally induced quantum interference. Phys. Rev. Lett.* **34**, 1472–1474.

Davidson, J. B. & Case, A. L. (1976). *Applications of the fly's eye neutron camera: diffraction tomography and phase transition studies. Proceedings of the Conference on Neutron Scattering, Gatlinburg, Tennessee*, USERDA CONF 760601-P2, 1124–1135. Oak Ridge, Tennessee: Oak Ridge National Laboratory.

Davidson, J. B., Werner, S. A. & Arrott, A. S. (1974). *Neutron microscopy of spin density wave domains in chromium. Proceedings of the 19th Annual Conference on Magnetism and Magnetic Materials*, edited by C. D. Graham and J. J. Rhyne. *AIP Conf. Proc.* **18**, 396–400.

Doi, K., Minakawa, N., Motohashi, H. & Masaki, N. (1971). *A trial of neutron diffraction topography. J. Appl. Cryst.* **4**, 528–530.

Eichhorn, F. (1988). *Perfect crystal neutron optics. Physica B*, **151**, 140–146.

Eichhorn, F., Sippel, D. & Kleinstück, K. (1967). *Influence of oxygen segregations in silicon single crystals on the halfwidth of the double-crystal rocking curve of thermal neutrons. Phys. Status Solidi*, **23**, 237–240.

Guigay, J. P. (1989). *On integrated intensities in Kato's statistical diffraction theory. Acta Cryst.* A**45**, 241–244.

Guigay, J. P. & Chukhovskii, F. N. (1992). *Reformulation of the dynamical theory of coherent wave propagation by randomly distorted crystals. Acta Cryst.* A**48**, 819–826.

Guigay, J. P. & Chukhovskii, F. N. (1995). *Reformulation of the statistical theory of dynamical diffraction in the case E = 0. Acta Cryst.* A**51**, 288–294.

Guigay, J. P. & Schlenker, M. (1979*a*). *Integrated intensities and flipping ratios in neutron diffraction by perfect magnetic crystals*. In *Neutron Interferometry*, edited by U. Bonse & H. Rauch, pp. 135–148. Oxford: Clarendon Press.

Guigay, J. P. & Schlenker, M. (1979*b*). *Spin rotation of the forward diffracted beam in neutron diffraction by perfect magnetic crystals. J. Magn. Magn. Mater.* **14**, 340–343.

Hart, M. & Rodrigues, A. R. D. (1978). *Harmonic-free single-crystal monochromators for neutrons and X-rays. J. Appl. Cryst.* **11**, 248–253.

Hastings, J. B., Siddons, D. P. & Lehmann, M. (1990). *Diffraction broadening and suppression of the inelastic channel in resonant neutron scattering. Phys. Rev. Lett.* **64**, 2030–2033.

Horne, M. A., Finkelstein, K. D., Shull, C. G., Zeilinger, A. & Bernstein, H. J. (1988). *Neutron spin – Pendellösung resonance. Physica B*, **151**, 189–192.

Indenbom, V. L. (1979). *Diffraction focusing of neutrons. JETP Lett.* **29**, 5–8.

International Tables for Crystallography (2004). Vol. C. *Mathematical, Physical and Chemical Tables*, edited by E. Prince. Dordrecht: Kluwer Academic Publishers.

Iolin, E. M. & Entin, I. R. (1983). *Dynamic diffraction of neutrons by high-frequency acoustic waves in perfect crystals. Sov. Phys. JETP*, **58**, 985–989.

Iolin, E. M., Zolotoyabko, E. V., Raïtman, E. A., Kuvdaldin, B. V. & Gavrilov, V. N. (1986). *Interference effects in dynamic neutron diffraction under conditions of ultrasonic excitation. Sov. Phys. JETP*, **64**, 1267–1271.

Kagan, Yu. & Afanas'ev, A. M. (1966). *Suppression of inelastic channels in resonance scattering of neutrons in regular crystals. Sov. Phys. JETP*, **22**, 1032–1040.

Kato, N. (1980*a*). *Statistical dynamical theory of crystal diffraction. I. General formulation. Acta Cryst.* A**36**, 763–769.

Kato, N. (1980*b*). *Statistical dynamical theory of crystal diffraction. II. Intensity distribution and integrated intensity in the Laue cases. Acta Cryst.* A**36**, 770–778.

Kikuta, S., Ishikawa, I., Kohra, K. & Hoshino, S. (1975). *Studies on dynamical diffraction phenomena of neutrons using properties of wave fan. J. Phys. Soc. Jpn*, **39**, 471–478.

Kikuta, S., Kohra, K., Minakawa, N. & Doi, K. (1971). *An observation of neutron Pendellösung fringes in a wedge-shaped silicon single crystal. J. Phys. Soc. Jpn*, **31**, 954–955.

Klar, B. & Rustichelli, F. (1973). *Dynamical neutron diffraction by ideally curved crystals. Nuovo Cimento B*, **13**, 249–271.

Klein, A. G. (1988). *Schrödinger inviolate: neutron optical searches for violations of quantum mechanics. Physica B*, **151**, 44–49.

Klein, A. G. & Werner, S. A. (1983). *Neutron optics. Rep. Prog. Phys.* **46**, 259–335.

Knowles, J. W. (1956). *Anomalous absorption of slow neutrons and X-rays in nearly perfect single crystals. Acta Cryst.* **9**, 61–69.

Korpiun, P. (1966). *Untersuchung ferromagnetischer Strukturen mit einem Zweistrahl-Neutroneninterferometer. Z. Phys.* **195**, 146–170.

Kulda, J. (1988*a*). *The RED extinction model. I. An upgraded formalism. Acta Cryst.* A**44**, 283–285.

Kulda, J. (1988*b*). *The RED extinction model. II. Refinement of extinction and thermal vibration parameters for SrF_2 crystals. Acta Cryst.* A**44**, 286–290.

Kulda, J. (1991). *The RED extinction model. III. The case of pure primary extinction. Acta Cryst.* A**47**, 775–779.

Kulda, J., Baruchel, J., Guigay, J.-P. & Schlenker, M. (1991). *Extinction effects in polarized neutron diffraction from magnetic crystals. I. Highly perfect MnP and YIG samples. Acta Cryst.* A**47**, 770–775.

Kulda, J., Vrána, M. & Mikula, P. (1988). *Neutron diffraction by vibrating crystals. Physica B*, **151**, 122–129.

Kvardakov, V. V., Podurets, K. M., Baruchel, J. & Sandonis, J. (1995). *Precision determination of the structure factors of magnetic neutron scattering from the Pendellösung data. Crystallogr. Rep.* **40**, 330–331.

Kvardakov, V. V., Podurets, K. M., Chistyakov, R. R., Shil'shtein, S. Sh., Elyutin, N. O., Kulidzhanov, F. G., Bradler, J. & Kadečková, S. (1987). *Modification of the domain structure of a silicon–iron single crystal as a result of uniaxial stretching. Sov. Phys. Solid State*, **29**, 228–232.

Kvardakov, V. V. & Somenkov, V. A. (1990). *Observation of dynamic oscillations of intensity of magnetic scattering of neutrons with variation of the orientation of magnetic moments of the sublattices. Sov. Phys. Crystallogr.* **35**, 619–622.

Kvardakov, V. V. & Somenkov, V. A. (1991). *Neutron diffraction study of nonlinear magnetoacoustic effects in perfect crystals of $FeBO_3$ and α-Fe_2O_3. J. Moscow Phys. Soc.* **1**, 33–57.

Kvardakov, V. V. & Somenkov, V. A. (1992). *Magnetic Pendellösung effects in neutron scattering by perfect magnetic crystals. Acta Cryst.* A**48**, 423–430.

Kvardakov, V. V., Somenkov, V. A. & Shil'shtein, S. Sh. (1990*a*). *Observation of dynamic oscillations in the temperature dependence of the intensity of the magnetic scattering of neutrons. Sov. Phys. Solid State*, **32**, 1097–1098.

Kvardakov, V. V., Somenkov, V. A. & Shil'shtein, S. Sh. (1990*b*). *Influence of an orientational magnetic transition in α-Fe_2O_3 on the Pendellösung fringe effect in neutron scattering. Sov. Phys. Solid State*, **32**, 1250–1251.

Kvardakov, V. V., Somenkov, V. A. & Shil'shtein, S. Sh. (1992). *Study of defects in cuprate single crystals by the neutron topography and selective etching methods. Superconductivity*, **5**, 623–629.

Lambert, D. & Malgrange, C. (1982). *X-ray and neutron integrated intensity diffracted by perfect crystals in transmission. Z. Naturforsch. Teil A*, **37**, 474–484.

Malgrange, C., Pétroff, J. F., Sauvage, M., Zarka, A. & Englander, M. (1976). *Individual dislocation images and Pendellösung fringes in neutron topographs. Philos. Mag.* **33**, 743–751.

Mendiratta, S. K. & Blume, M. (1976). *Dynamical theory of thermal neutron scattering. I. Diffraction from magnetic crystals. Phys. Rev.* **14**, 144–154.

Michalec, R., Mikula, P., Sedláková, L., Chalupa, B., Zelenka, J., Petržílka, V. & Hrdlička, Z. (1975). *Effects of thickness-shear vibrations on neutron diffraction by quartz single crystals. J. Appl. Cryst.* **8**, 345–351.

Michalec, R., Mikula, P., Vrána, M., Kulda, J., Chalupa, B. & Sedláková, L. (1988). *Neutron diffraction by perfect crystals excited into mechanical resonance vibrations. Physica B*, **151**, 113–121.

Podurets, K. M., Sokol'skii, D. V., Chistyakov, R. R. & Shil'shtein, S. Sh. (1991). *Reconstruction of the bulk domain structure of silicon iron single crystals from neutron refraction images of internal domain walls. Sov. Phys. Solid State*, **33**, 1668–1672.

Podurets, K. M., Somenkov, V. A., Chistyakov, R. R. & Shil'shtein, S. Sh. (1989). *Visualization of internal domain structure of silicon iron crystals by using neutron radiography with refraction contrast. Physica B*, **156–157**, 694–697.

Podurets, K. M., Somenkov, V. A. & Shil'shtein, S. Sh. (1989). *Neutron radiography with refraction contrast. Physica B*, **156–157**, 691–693.

Rauch, H. (1995). *Towards interferometric Fourier spectroscopy. Physica B*, **213–214**, 830–832.

Rauch, H. & Petrascheck, D. (1978). *Dynamical neutron diffraction and its application*. In *Neutron Diffraction*, edited by H. Dachs, *Topics in Current Physics*, Vol. 6 pp. 305–351. Berlin: Springer.

Rauch, H. & Seidl, E. (1987). *Neutron interferometry as a new tool in condensed matter research. Nucl. Instrum. Methods A*, **255**, 32–37.

Raum, K., Koellner, M., Zeilinger, A., Arif, M. & Gähler, R. (1995). *Effective-mass enhanced deflection of neutrons in noninertial frames. Phys. Rev. Lett.* **74**, 2859–2862.

Scherm, R. & Fåk, B. (1993). *Neutrons*. In *Neutron and Synchrotron Radiation for Condensed Matter Studies (HERCULES Course)*, Vol. 1, edited by J. Baruchel, J. L. Hodeau, M. S. Lehmann, J. R. Regnard & C. Schlenker, pp. 113–143. Les Ulis: Les Editions de Physique and Heidelberg: Springer-Verlag.

Schlenker, M. & Baruchel, J. (1978). *Neutron techniques for the observation of ferro- and antiferromagnetic domains. J. Appl. Phys.* **49**, 1996–2001.

Schlenker, M., Baruchel, J., Perrier de la Bathie, R. & Wilson, S. A. (1975). *Neutron-diffraction section topography: observing crystal slices before cutting them. J. Appl. Phys.* **46**, 2845–2848.

Schlenker, M., Baruchel, J., Pétroff, J. F. & Yelon, W. B. (1974). *Observation of subgrain boundaries and dislocations by neutron diffraction topography. Appl. Phys. Lett.* **25**, 382–384.

Schlenker, M., Bauspiess, W., Graeff, W., Bonse, U. & Rauch, H. (1980). *Imaging of ferromagnetic domains by neutron interferometry. J. Magn. Magn. Mater.* **15–18**, 1507–1509.

Schlenker, M., Linares-Galvez, J. & Baruchel, J. (1978). *A spin-related contrast effect: visibility of 180° ferromagnetic domain walls in unpolarized neutron diffraction topography. Philos. Mag. B*, **37**, 1–11.

Schlenker, M. & Shull, C. G. (1973). *Polarized neutron techniques for the observation of ferromagnetic domains. J. Appl. Phys.* **44**, 4181–4184.

Schmidt, H. H. (1983). *Theoretical investigations of the dynamical neutron diffraction by magnetic single crystals. Acta Cryst.* A**39**, 679–682.

Schmidt, H. H., Deimel, P. & Daniel, H. (1975). *Dynamical diffraction of thermal neutrons by absorbing magnetic crystals. J. Appl. Cryst.* **8**, 128–131.

Sears, V. F. (1978). *Dynamical theory of neutron diffraction. Can. J. Phys.* **56**, 1261–1288.

Shil'shtein, S. Sh., Somenkov, V. A. & Dokashenko, V. P. (1971). *Suppression of (n, γ) reaction in resonant scattering of neutrons by a perfect CdS crystal. JETP Lett.* **13**, 214–217.

Shull, C. G. (1968). *Observation of Pendellösung fringe structure in neutron diffraction. Phys. Rev. Lett.* **21**, 1585–1589.

Shull, C. G. (1986). *Neutron interferometer systems – types and features. Physica B*, **136**, 126–130.

Shull, C. G. & Oberteuffer, J. A. (1972). *Spherical wave neutron propagation and Pendellösung fringe structure in silicon. Phys. Rev. Lett.* **29**, 871–874.

Shull, C. G., Zeilinger, A., Squires, G. L., Horne, M. A., Atwood, D. K. & Arthur, J. (1980). *Anomalous flight time of neutrons through diffracting crystals. Phys. Rev. Lett.* **44**, 1715–1718.

Sippel, D. & Eichhorn, F. (1968). *Anomale inkohärente Streuung thermicher Neutronen bei Bildung stehender Neutronenwellen in nahezu idealen Kristallen von Kaliumdihydrogenphosphat (KDP). Acta Cryst.* A**24**, 237–239.

Sippel, D., Kleinstück, K. & Schulze, G. E. R. (1962). *Nachweis der anomalen Absorption thermischer Neutronen bei Interferenz am Idealkristall. Phys. Status Solidi*, **2**, K104–K105.

Sippel, D., Kleinstück, K. & Schulze, G. E. R. (1964). *Neutron diffraction of ideal crystals using a double crystal spectrometer. Phys. Lett.* **8**, 241–242.

Sippel, D., Kleinstück, K. & Schulze, G. E. R. (1965). *Pendellösungs-Interferenzen mit thermischen Neutronen an Si-Einkristallen. Phys. Lett.* **14**, 174–175.

Sivardière, J. (1975). *Théorie dynamique de la diffraction magnétique des neutrons. Acta Cryst.* A**31**, 340–344.

Somenkov, V. A., Shil'shtein, S. Sh., Belova, N. E. & Utemisov, K. (1978). *Observation of dynamical oscillations for neutron scattering by Ge crystals using the inclination method. Solid State Commun.* **25**, 593–595.

Squires, G. L. (1978). *Introduction to the Theory of Thermal Neutron Scattering*. Cambridge University Press.

Stassis, C. & Oberteuffer, J. A. (1974). *Neutron diffraction by perfect crystals. Phys. Rev. B*, **10**, 5192–5202.

Takagi, S. (1962). *Dynamical theory of diffraction applicable to crystals with any kind of small distortion. Acta Cryst.* **15**, 1311–1312.

Takahashi, T., Tomimitsu, H., Ushigami, Y., Kikuta, S. & Doi, K. (1981). *The very-small angle neutron scattering from neutron-irradiated amorphous silica. Jpn. J. Appl. Phys.* **20**, L837–L839.

Takahashi, T., Tomimitsu, H., Ushigami, Y., Kikuta, S., Doi, K. & Hoshino, S. (1983). *The very-small angle neutron scattering from SiO_2–PbO glasses. Physica B*, **120**, 362–366.

Tasset, F. (1989). *Zero field neutron polarimetry. Physica B*, **156–157**, 627–630.

Taupin, D. (1964). *Théorie dynamique de la diffraction des rayons X par les cristaux déformés. Bull. Soc. Fr. Minéral. Cristallogr.* **87**, 469–511.

Tomimitsu, H. & Doi, K. (1974). *A neutron diffraction topographic observation of strain field in a hot-pressed germanium crystal. J. Appl. Cryst.* **7**, 59–64.

Tomimitsu, H., Doi, K. & Kamada, K. (1983). *Neutron diffraction topographic observation of substructures in Cu-based alloys. Physica B*, **120**, 96–102.

Tomimitsu, H., Takahashi, T., Kikuta, S. & Doi, K. (1986). *Very small angle neutron scattering from amorphous $Fe_{78}B_{12}Si_{10}$. J. Non-Cryst. Solids*, **88**, 388–394.

Tomimitsu, H. & Zeyen, C. (1978). *Neutron diffraction topographic observation of twinned silicon crystal. Jpn. J. Appl. Phys.* **3**, 591–592.

Werner, S. A. (1980). *Gravitational and magnetic field effects on the dynamical diffraction of neutrons. Phys. Rev. B*, **21**, 1774–1789.

Werner, S. A. (1995). *Neutron interferometry tests of quantum theory. Ann. NY Acad. Sci.* **755**, 241–262.

Werner, S. A., Staudenmann, J. L. & Colella, R. (1979). *The effect of the Earth's rotation on the quantum mechanical phase of the neutron. Phys. Rev. Lett.* **42**, 1103–1106.

Zachariasen, W. H. (1967). *A general theory of X-ray diffraction in crystals. Acta Cryst.* **23**, 558–564.

Zeilinger, A. (1995). Private communication.

Zeilinger, A. & Shull, C. G. (1979). *Magnetic field effects on dynamical diffraction of neutrons by perfect crystals. Phys. Rev. B*, **19**, 3957–3962.

Zeilinger, A., Shull, C. G., Horne, M. A. & Finkelstein, K. D. (1986). *Effective mass of neutrons diffracting in crystals. Phys. Rev. Lett.* **57**, 3089–3092.

Zelepukhin, M. V., Kvardakov, V. V., Somenkov, V. A. & Shil'shtein, S. Sh. (1989). *Observation of the Pendellösung fringe effect in magnetic scattering of neutrons. Sov. Phys. JETP*, **68**, 883–886.

Zolotoyabko, E. & Sander, B. (1995). *X-ray diffraction profiles in strained crystals undergoing ultrasonic excitation. The Laue case. Acta Cryst.* A**51**, 163–171.